

**A QUANTIFIED BAYESIAN MAXIMUM ENTROPY ESTIMATE OF  
ANTARCTIC KRILL ABUNDANCE ACROSS THE SCOTIA SEA  
AND IN SMALL-SCALE MANAGEMENT UNITS  
FROM THE CCAMLR-2000 SURVEY**

B.G. Heywood✉ and A.S. Brierley  
Pelagic Ecology Research Group  
Gatty Marine Laboratory  
University of St Andrews  
Fife KY16 8LB, United Kingdom  
Email – bgh@st-and.ac.uk

S.F. Gull  
Astrophysics Group  
Cavendish Laboratory  
University of Cambridge  
Madingley Road  
Cambridge, CB3 0HE  
United Kingdom

Abstract

A probabilistic Bayesian Maximum Entropy (MaxEnt) technique was used to estimate the abundance of Antarctic krill (*Euphausia superba*) across the Scotia Sea using data from the CCAMLR 2000 Krill Synoptic Survey of Area 48 (CCAMLR-2000 Survey) and to map the density distribution of krill across the survey area. Density values for the unsurveyed off-transect portions of the survey area were inferred, and thus values for total biomass across the survey area, and within individual small-scale management units (SSMUs), were estimated. Abundance in some of the individual SSMUs had not previously been estimated due to the sparseness of data in these regions. The MaxEnt formalism allows an objective choice of the parameters of the estimation method, and hence an objective choice of the most probable reconstruction of krill distribution, given the data. The Bayesian framework also allows intrinsic calculation of the error in the density estimates. The total biomass inferred for the survey area was 208 million tonnes, with a standard deviation of 10 million tonnes. The MaxEnt method provides new insights into the extremely sparse survey data (only 0.6% of the survey area was directly acoustically sampled), and enhances the conservation and management potential of the CCAMLR-2000 Survey.

Résumé

Une technique probabiliste bayésienne de maximum d'entropie (MaxEnt) a permis d'estimer l'abondance du krill antarctique (*Euphausia superba*) dans l'ensemble de la mer du Scotia à partir des données de la campagne CCAMLR-2000 d'évaluation synoptique du krill de la zone 48 (campagne CCAMLR-2000) et de tracer la distribution de la densité du krill de toute la région couverte par la campagne. Les valeurs de densité pour les portions hors transects, et donc non évaluées, de la campagne d'évaluation ont été inférées et, de ce fait, les valeurs de la biomasse totale de cette région et de chacune des unités de gestion à petite échelle (SSMU) ont été estimées. L'abondance, dans certaines SSMU, n'avait jamais été estimée en raison du peu de données disponibles sur ces régions. Le formalisme de MaxEnt permet un choix objectif des paramètres de la méthode d'estimation et, de ce fait, de la reconstruction la plus probable de la répartition du krill, compte tenu des données. La structure bayésienne permet également le calcul intrinsèque de l'erreur des estimations de densité. La biomasse totale inférée pour la zone couverte par la campagne était de 208 millions de tonnes, pour un écart-type de 10 millions de tonnes. La méthode MaxEnt offre un éclaircissement à l'égard des données extrêmement limitées de la campagne (lorsque 0,6% seulement de la zone couverte a fait l'objet d'une évaluation acoustique directe) et augmente les possibilités de conservation et de gestion offertes par la campagne CCAMLR-2000.

Резюме

Для оценки численности антарктического криля (*Euphausia superba*) в море Скотия по данным синоптической съемки криля, проводившейся АНТКОМом в 2000 г. в Районе 48 (съемка АНТКОМ-2000), и для составления карты распределения

плотности криля в районе съемки использовался вероятностный байесовский максимально энтропийный (MaxEnt) метод. Были получены значения плотности для необследованных частей съемочного района за пределами разрезов и, таким образом, оценены значения общей биомассы в районе съемки и в отдельных мелкомасштабных единицах управления (SSMU). Численность в нескольких отдельных SSMU ранее не оценивалась из-за недостаточного количества данных по этим районам. Формализм MaxEnt допускает объективный выбор параметров метода оценки и, тем самым, объективный выбор наиболее вероятной реконструкции распределения криля с учетом данных. Байесовская концепция также допускает характеристический расчет ошибки в оценках плотности. Полученная общая биомасса в районе съемки составила 208 млн. т со стандартным отклонением 10 млн. т. Метод MaxEnt позволяет по-новому взглянуть на чрезвычайно скудные съемочные данные (непосредственный сбор акустических данных проводился только в 0.6% района съемки) и повышает природоохранное и управленческое значение съемки АНТКОМ-2000.

#### Resumen

Se utilizó un método probabilístico Bayesiano de máxima entropía (MaxEnt) para estimar la abundancia de kril antártico (*Euphausia superba*) en el Mar de Escocia a partir de los datos de la prospección sinóptica de kril CCAMLR 2000 realizada en el Área 48, y para graficar la distribución de las densidades de kril en el área de prospección. Los valores de la densidad para la proporción del área de prospección que no fue cubierta por los transectos fueron inferidos, estimándose de esta manera el total de la biomasa en el área de prospección, y dentro de cada unidad de ordenación en pequeña escala (UOPE). No se había estimado anteriormente la abundancia de algunas UOPE debido a la escasez de datos de estas regiones. El método de MaxEnt permite seleccionar objetivamente los parámetros del método de estimación, y por consiguiente, elegir objetivamente la reconstrucción más probable de la distribución de kril, dados los datos de los cuales se dispone. Asimismo, el análisis Bayesiano permite efectuar un cálculo intrínseco del error de las estimaciones de la densidad. La biomasa total inferida para el área de prospección fue de 208 millones de toneladas, con una desviación estándar de 10 millones de toneladas. El método de MaxEnt revela nuevos aspectos de los datos, extremadamente escasos, de la prospección (solamente se tomaron muestras acústicas de un 0.6% del área de prospección), y aumenta el potencial de la prospección CCAMLR-2000 para la conservación y ordenación.

Keywords: Maximum Entropy, *Euphausia superba*, acoustic, Bayes, SSMU, CCAMLR

#### Introduction

The CCAMLR 2000 Krill Synoptic Survey of Area 48 (CCAMLR-2000 Survey) (Trathan et al., 2001; Hewitt et al., 2004a) of the Scotia Sea employed acoustic techniques to measure the density distribution of Antarctic krill. Due to inevitable pressures of time and expense, only a very small fraction (0.56%) of the total survey area was acoustically sampled directly, and hence some method of estimating total abundance from these limited data is necessary. Hewitt et al. (2002) used the Jolly and Hampton (1990) statistical method and calculated a total biomass across the survey area of 44.3 million tonnes. The Jolly and Hampton method involves generating weighted means for a number of semi-randomly placed transects, and the CCAMLR-2000 Survey was designed in accordance with such transect placing. Demer and Conti (2005) used the same method, but their updated krill target-strength model led to a biomass estimate of 109.4 million tonnes. This paper presents a biomass estimate, based on the Demer and Conti (2005)

target-strength model, derived using a Bayesian Maximum Entropy (MaxEnt) technique rather than the standard Jolly and Hampton (1990) method. MaxEnt maps of the density distribution are presented as an alternative to the standard kriged maps (a good description of the kriging approach can be found in Rivoirard et al. (2000)) of density distribution, as given by Hewitt et al. (2004a).

In addition to the survey total, biomass estimates derived by the MaxEnt method for each of the krill small-scale management units (SSMUs – Hewitt et al. 2004b – see Table 1 and Figure 1) are presented. These SSMUs are ecologically crucial areas around South Georgia, the South Orkney Islands and the South Shetland Islands within which land-based predators forage, and are likely to be particularly important from an ecosystem management perspective. Since the densities estimated by the Jolly and Hampton (1990) method are per stratum of the survey, previous estimates of biomass within certain SSMUs have been based on the density determined for nearby strata (Hewitt et al., 2004b),

Table 1: List of SSMU designations.

SSMU	Number	Full title
APPA	1	Antarctic Peninsula Pelagic Area (Subarea 48.1)
APW	2	Antarctic Peninsula West
APDPW	3	Drake Passage West
APDPE	4	Drake Passage East
APBSW	5	Bransfield Strait West
APBSE	6	Bransfield Strait East
APEI	7	Elephant Island
APE	8	Antarctic Peninsula East
SOPA	9	South Orkney Pelagic Area (Subarea 48.2)
SOW	10	South Orkney West
SONE	11	South Orkney North East
SOSE	12	South Orkney South East
SGPA	13	South Georgia Pelagic Area (Subarea 48.3)
SGW	14	South Georgia West
SGE	15	South Georgia East
	16	Subarea 48.4

despite the fact that only parts of these strata fall within the SSMUs. The density distribution maps generated by MaxEnt enable biomass values for the SSMUs to be inferred on a more appropriate spatial scale.

The MaxEnt image reconstruction method has been widely and successfully used to generate complete images from sparse point data in many disciplines, from astrophysics (e.g. Weir and Djorgovski, 1991) to medicine (e.g. Charter and Gull, 1991). The inference of krill density values in grid squares across the CCAMLR-2000 Survey area can be treated as an exercise in image reconstruction, since the data consist of point estimates of krill density derived from echo integration at a given latitude and longitude, and hence the data space is two-dimensional. A set of point values on a two-dimensional grid can naturally be viewed as a pixellated image or picture. The problem of filling in missing data is then directly analogous to the problem of reconstructing a damaged photograph, or improving the resolution of astronomical images, and therefore reconstruction techniques from these disciplines may sensibly be applied to these biological data. The CCAMLR-2000 Survey data can be considered as an image in which krill densities are plotted on a rectangular grid, with correspondingly brighter dots for higher density values. A reconstruction of the missing parts of this image grid is then attempted, in order to create a map from which total biomass can be estimated. The intensity of each pixel in the reconstructed image corresponds to an estimate of krill density ( $\text{g m}^{-2}$ ) in that pixel, where each pixel represents a 1 n mile  $\times$  1 n mile cell of the survey area. MaxEnt image reconstruction has previously been used

to generate maps and biomass estimates from smaller-scale surveys of krill around South Georgia (Brierley et al., 2003; Wafy et al., 2003).

Line-transect data contain potentially valuable information on spatial distribution, which is ignored by conventional statistical techniques (e.g. Jolly and Hampton, 1990). It is assumed that the MaxEnt method offers advantages over the Jolly and Hampton (1990) method because it makes explicit use of this spatial information (Brierley et al., 2003). The other commonly used techniques for biomass estimation are geostatistical (Rivoirard et al., 2000), but Maravelias et al. (1996) showed that such methods are unsatisfactory when the distribution of biomass is heavily skewed, which is very much the case with the krill density data from the CCAMLR-2000 Survey. Densities of almost  $24\,000\text{ g m}^{-2}$  were reported for individual 1 n mile<sup>2</sup> regions, but only 0.8% of measurements exceeded  $1\,000\text{ g m}^{-2}$ , and two-thirds were under  $10\text{ g m}^{-2}$  (see Figure 2).

## Methods

### What is Maximum Entropy image reconstruction?

Image reconstruction, in this case, is the inference of missing values in a grid framework. MaxEnt describes the statistical probabilistic framework under which this is achieved. Johnson and Shore (1980, 1983) and Tikochinsky et al. (1984) offer clear theoretical and mathematical justifications for the use of MaxEnt, and the method has been placed robustly in a rigorous Bayesian framework (Skilling, 1988a; Skilling and Gull, 1989; Skilling

and Sibisi, 1990; Gull and Skilling, 1991; Skilling, 1991; see Sivia, 1996 for an introduction to Bayesian data analysis; and Clark, 2005 on why ecologists are becoming Bayesians). This paper presents just one relatively non-mathematical argument for the use of MaxEnt (drawn from Skilling, 1992), and concentrates on its application to biomass estimation and distribution mapping from fishery acoustic data.

Bayes' theorem (Bayes, 1763; Cox, 1946; Jaynes, 2003) is used:

$$\text{prob}(\mathbf{h} | \text{data}) \propto \text{prob}(\mathbf{h}) \text{prob}(\text{data} | \mathbf{h})$$

where ' $|$ ' means 'given', and  $\mathbf{h}$  is the set of all possible images (i.e. krill distributions)  $h$ , each consisting of the intensity (i.e. density) values in  $m$  pixels (i.e. 1 n mile  $\times$  1 n mile cells of the survey area),  $h_1, h_2 \dots h_m$ . The posterior inference  $\text{prob}(\mathbf{h} | \text{data})$  measures how closely trial images  $h$  are in accord with the survey data, given any prior information,  $\text{prob}(\mathbf{h})$ . The other factor,  $\text{prob}(\text{data} | \mathbf{h})$ , is the Bayesian Likelihood. Since noise in the data can tolerably be described by Gaussian statistics (Gull and Skilling, 1991), a Gaussian likelihood function is adequate (Gull and Skilling, 1991).

To use the above formula, a sensible prior distribution of images,  $\text{prob}(\mathbf{h})$ , needs to be assigned. This specifies one's original ideas, without the data, about the plausibility of various images  $h$ . A prior according to the principle of MaxEnt (Jaynes, 1978) was chosen. One relatively non-technical explanation of why the concept of entropy should be fundamental to the process is as follows:

Suppose an enormous number  $N$  of individual krill are thrown, one by one and at random, into an empty Scotia Sea, which has been conveniently split into 1 n mile  $\times$  1 n mile cells. This imaginary experiment is repeated many times. The aim is to quantify the preferences for different possible distributions of krill, without reference to (i.e. prior to) any data. Fortunately, not all distributions are equal – some are more probable than others. For example, a total of seven is the most likely outcome of the roll of two dice, even though the value on each die is completely random, because there are more ways to make seven from two dice than any other number. Similarly, there are more ways of distributing the krill evenly across of the Scotia Sea (i.e. an equal number in each 1 n mile  $\times$  1 n mile cell) than there are of distributing them in any particular uneven pattern. In fact, the prior probability of any particular pattern being produced is

proportional to the number of permutations  $\Omega$  of  $N$  krill that result in that particular pattern, which is given by

$$\Omega(n) = \frac{N!}{n_1!n_2!\dots n_m!}$$

where  $n_1 \dots n_m$  are the numbers of krill in cells 1, 2, ...  $m$ .

It is mathematically much more convenient to work with the logarithm of  $\Omega$ , called the *entropy*,  $S$ .

$$S = \log \Omega \approx \sum n_i \log n_i.$$

The prior expectation,  $\text{prob}(\mathbf{h})$ , incorporating the expectation of randomness and unpredictability (which expresses the lack of prior knowledge) can – after some mathematical work (see Skilling, 1992) which is beyond the scope of this paper – be written in terms of the entropy  $S$  as

$$\text{prob}(\mathbf{h}) \propto \exp(S).$$

This is an entropy-based prior distribution which expresses a preference for smoothness (since an equal distribution of krill across all cells has the highest number of permutations). A more rigorous mathematical approach (Skilling, 1988a, 1988b) confirms and justifies this result, and properly calculates the scaling constants to remove the proportionality.

Using the chosen prior and likelihood, it is now possible to calculate the most probable posterior image by means of Bayes' theorem. This most probable image is the traditional MaxEnt result. However, since the prior is a probability *distribution* of images, so is the posterior; in fact it is possible not only to calculate the maximum of the posterior distribution (the most probable image), but also to sample, from the posterior probability space, a selection of the images near that maximum. This then enables calculation of the standard deviation of each pixel in the reconstruction. This is the quantified MaxEnt result.

#### Parameter estimation

Each image reconstruction requires the choice of a small number of parameters, for example the width of the blurring function, described below, which is used to capture spatial autocorrelation in the data. Crucially, the normalising constant of Bayes' theorem, a value which is often known as the *evidence*,  $P(\text{data})$ , can be calculated for each set of parameters:

$$P(\text{data}) = \sum_h \text{prob}(\mathbf{h}, \text{data})$$

where  $\mathbf{h}$  now contains only those images consistent with the chosen parameters.  $P(\text{data})$  is used to indicate that this is a single probability value (rather than a distribution) calculated from a particular reconstruction attempt with particular input parameters. The evidence value is a unitless probability between zero and one, and is usually presented as its logarithm.

The evidence value is used to discriminate between prior images, much as the likelihood discriminates between posterior images (Gull and Skilling, 1991). Note that the prior distribution  $\text{prob}(\mathbf{h})$  is a *distribution of prior images*, and not an individual prior image. This distribution  $\text{prob}(\mathbf{h})$  tells us which images are more likely in advance – before the data – and the comparison of a number of values for evidence tells us which selection of prior images, defined as those consistent with the chosen parameters, produced the most likely MaxEnt result, after considering the data.

By running a number of reconstructions with different parameters (i.e. different *assumed* prior information, in effect a different set of prior images), and choosing the one with the highest evidence value, the optimal values of any unknown parameters can be progressively approached.

The use of the evidence value to decide objectively between possible parameter values is a major strength of MaxEnt. The chosen reconstruction must be that with the highest evidence, regardless of the prejudices of the researcher. This applies to any alterable parameter of the reconstruction, not only those estimated in this paper but also more fundamental elements such as the shape of the blurring function discussed below.

The analysis was undertaken using the software MemSys5 (Gull and Skilling, 1991).

#### Calculating the quantified MaxEnt result

The data gathered by an acoustic survey of a defined area are usually, like almost all data, incomplete. This is certainly the case for the CCAMLR-2000 Survey. There is in principle no mathematical transform that can be applied to the data that will result in the actual krill densities in every ‘pixel’ since there is not enough information in the data – data cannot be transformed to image. Therefore, it is necessary to approach the problem from the other direction – by generating a trial image (in

this case a possible krill density distribution across the whole survey area) and transforming this into mock data (the set of on-transect values implied by this trial density distribution). After comparing this with the actual data, another trial image is generated, which has been updated so that the next mock dataset will be a better fit.

The first trial image is simply the uniform image. This is the most likely distribution in the absence of data. Since the final image evolves from this smooth starting point, any structure in the reconstructed image must be introduced by the data itself, and cannot be an artefact of the first trial image. This smooth starting image is then iteratively updated by comparison with the data (i.e. the on-transect density values from Demer and Conti (2005)), and becomes progressively less smooth. The iterations stop when the fit of the mock data (from the latest trial image) to the actual data is optimal, where optimal is defined in terms of the balance between the entropy (which decreases as one moves away from the completely smooth image) and the likelihood (which increases as the fit to the data becomes more exact). This balance between entropy (upon which the prior distribution is based) and likelihood is directly analogous to the formulation of Bayes’ theorem above. Stopping the iterative process too soon will mean that some genuine data are not fitted, and stopping too late will mean that noise in the data begin to be fitted, resulting in unwarranted structure in the reconstruction. The MaxEnt stopping criterion is chosen on solid mathematical and probabilistic grounds (Gull and Skilling, 1991).

The transform applied to generate the mock data from a trial image depends heavily on the particular application of the MaxEnt method. In astrophysics, for example, the data from an instrument may be a Fourier transform of the real-world image, and therefore such a transform would need to be applied to each trial image in order to approach the correct result. Similarly, complex transforms are sometimes necessary with biological data. Lizamore (1995) used commercial trawl data to reconstruct density distributions for New Zealand hoki. A transform between data space (trawl length and position, weight of catch) and image space (density in each pixel) was required.

In the application of MaxEnt to fishery acoustic surveys, there is no need for such complication, since both the data and the image reside in the same mathematical space and share the same units. Thus, the only transform applied between image and data is a blurring function, which characterises

the expectation that, on biological grounds, some local smoothness (spatial autocorrelation) should exist in the final image (Weber et al., 1986).

The blurring function used here is simply an approximation to a Gaussian point spread function. It is necessary to choose a width for this blur, and it has been found that in practice a particular smoothing width tends to emphasise structure of a similar width in the reconstruction. Since it is reasonable to expect local structure (in this case, krill swarms and/or clusters of swarms) to have varying sizes, this is unwelcome. The solution proposed by Weir and Djorgovski (1991), subsequently incorporated into MemSys5, is to concurrently produce a number of 'hidden' reconstructions, each with a different blurring width. These separate but concurrent reconstruction 'channels' are then convolved to produce a single image. Generally, precedent has suggested that each separate hidden reconstruction should have a blurring width twice as wide, and a weighting for the convolution four times smaller than (i.e. one quarter as much as) the previous hidden channel (which is termed a *scaling factor* for the blur equal to *two*, and a *weighting factor* for the convolution equal to *four*). Thus with four hidden reconstructions, the blurring widths would be 1, 2, 4 and 8 units, and the second, third and fourth channels would be 4, 16 and 64 times less important to the convolved reconstruction than the first channel.

Previous papers (Brierley et al., 2003; Wafy et al., 2003) used these essentially ad hoc values (for the scaling and weighting of hidden channels) for their reconstructions of krill density around South Georgia. However, the evidence value, as described above, can be used objectively to select not just the *number* of hidden channels (as Brierley and Wafy used it) but also objectively to select appropriate scaling and weighting. Recent changes, implemented to the software interface used to perform MaxEnt, mean that these values can be chosen at run-time. This has enabled much deeper exploration of the effect of these values than was available to the authors of these previous papers.

The standard deviation for each pixel value can be calculated under MaxEnt. A sampling of the posterior distribution generates a number of images, all very nearly as probable as the best estimate, but not necessarily similar in shape or total intensity. Stable, well-predicted pixels will be very similar in almost every reconstruction, whereas those about which greater uncertainty exists will fluctuate. For each pixel, there is therefore a population of values (one from each sample image) from which standard deviation (in  $\text{g m}^{-2}$ ) can very simply be calculated.

From these individual pixel standard deviations, the standard deviation of a given region or of the whole survey is simply the sum of the standard deviations of the pixels within it.

#### Data preparation

The on-transect data used here are exactly as used by Demer and Conti (2005) to calculate a 109.4 million tonne krill biomass estimate. In order to process the data as an image (a rectangular image, in fact, for ease of computation) it was necessary first to convert the positional stamps for this data (Demer and Conti, 2005) from latitude-longitude format to Cartesian (x,y) format so that a consistent spatial scale existed across the grid. A Lambert Conformal Conic projection was used. The coordinates defining the survey bounds and the SSMUs, identical to those used by Hewitt et al. (2002, 2004a, 2004b), were transformed by the same projection, so that the biomass inferred for any area could easily be found by summing the biomass of all pixels in that area. (Pixel biomass is  $1852^2 \text{ m}^2 \times \text{density (g m}^{-2}\text{)}$ , divided by  $10^{12}$  to convert from grams to million tonnes.) For those SSMUs that extend beyond the bounds of the survey, this method cannot be applied; instead the mean biomass of the pixels within these areas was multiplied by the total area of the SSMU, using the same SSMU area data as Hewitt et al. (2004b). Both these methods were applied to the SSMUs around South Georgia to check that the simple summing of pixel biomass did not induce any systematic bias. The estimates generated by the two methods differed by no more than 1%.

In addition, since the density data were extremely heavily skewed (see Figure 2), much better evidence values were obtained by normalising the distribution of the data somewhat before input to the algorithm. This is due to the normal shape of both the likelihood function and the blurring function, which naturally act more evenly on data with a normal-shaped distribution. Therefore, the second root of the density ( $\sqrt{\sqrt{\text{data}}}$ ) was input to the algorithm, and the result was squared twice before output. It should be noted that proponents of the kriging technique have also used data transforms to reduce the skew of the input data (Rivoirard et al., 2000); both kriging and MaxEnt are similarly challenged by skewed data and have developed similar solutions to the problem. Further experiments with the shape of the blurring function, which have not yet been undertaken, may reduce the need for such measures under MaxEnt.

## Results

Approximately 200 reconstructions were undertaken in total, and some statistics relating to a selection of these are presented in Table 2. The two parameters that had most effect on the reconstructed result were the number of hidden channels and the weighting factor (the rate of change of convolution weighting from one hidden channel to the next). The scaling factor (the rate of change of the blurring width) was found to have almost no effect on the result. Of the abovementioned reconstructions, 100 were therefore undertaken with all integer values of weighting factor 1 to 10 for all numbers of hidden channels 1 to 10 (each with an arbitrary scaling factor of two), although they are not all shown here, in order to check for possible multiple maxima of evidence. Figures 3 and 4 show some sample reconstructions created in order to assign values to these parameters. In fact, the distribution of evidence values for the reconstructions was well behaved and had a single peak, corresponding to eight hidden channels and a weighting factor of seven. This is the most probable MaxEnt reconstruction and is shown in Figure 5. For comparison, a previously published kriged estimate of density distribution from the CCAMLR-2000 Survey is reproduced in Figure 6.

The total krill biomass estimate from this result is 207.98 million tonnes, with a standard deviation of 10.08 million tonnes. Biomass estimates from this result are given for each of the 16 SSMUs (Figure 1) in Table 3. The standard deviations calculated for each individual pixel value of the image are shown in Figure 7. For some pixels the predicted standard deviation may be larger than the predicted biomass, thereby apparently suggesting the possibility of a negative biomass in that pixel, which is obviously impossible. This is a common problem with noisy data, and may in the case of MaxEnt also be related to a local failure of the Gaussian approximation to  $\text{prob}(h|\text{data})$  that is used in the calculation of standard deviation (Gull and Skilling, 1991).

It is prudent to note, when looking at the biomass and standard deviation values, that issues of calibration, target strength, krill orientation, species identification, sea-bottom detection etc., whilst of great importance to the final biomass and error estimates, lie beyond the scope of this paper – the authors merely wish, given previously calculated on-transect density values, to reconstruct the most probable off-transect distribution. For a discussion and calculation of the errors involved in the gathering and processing of the CCAMLR-2000 Survey data, see Demer (2004).

Even with this exceptionally large data space ( $1\,578 \times 1\,094 = 1\,726\,332$  pixels, of which data are available for 9 586 pixels or just 0.56%), results were obtained in 30–40 iterations of the algorithm, taking in total around 40 minutes on a 2.8 GHz Pentium 4 PC running Windows 2000. This is a sufficiently short time to allow the processing of the number of reconstructions needed to identify the image with the best evidence. Very thorough attention was paid to creating a wide range of possible reconstructions in order to ensure that the chosen result was indeed justified. However, the authors' experience with this data has supported the expectation that there is a single maximum for evidence (Gull and Skilling, 1991). This being the case, there is no need to continue to increase or decrease parameters such as weighting factor after a maximum has been passed, and very many fewer reconstructions are required to choose a result. Therefore, for confident reconstructions of, for example, images from any subsequent survey of CCAMLR Area 48 with a similar extent of data coverage, 10 to 15 reconstructions would be sufficient.

Direct testing of the quality of the reconstruction is not straightforward, since the 'truth' of the off-transect distribution of krill density is not and cannot be known. Concurrent with this work on the CCAMLR-2000 Survey data, however, is an investigation of the success of the MaxEnt technique in recreating a simulated dataset (based on the distribution of herring in the North Sea – Simmonds, Fernandes and Reid, pers. comm.). Although the area of this reconstruction from simulated data is very much smaller than the reconstruction area of the CCAMLR data ( $50\,625$  n miles<sup>2</sup> as opposed to  $1\,726\,332$  n miles<sup>2</sup>), the data are integrated on a much finer scale (440 m as opposed to 1 n mile), and hence the reconstruction of  $1\,024 \times 896$  pixels is similar in magnitude to the  $1\,578 \times 1\,094$  pixel reconstruction of the CCAMLR-2000 Survey data. Values are known for every pixel in this simulated dataset, and hence distributions reconstructed from virtual surveys along imaginary transects can be compared with the 'true' distribution. Many different virtual surveys can be generated, covering a higher or lower percentage of the total data space, with different transect spacing and orientation, and with different levels of noise added to the data, and so on. The preliminary results of this work so far show that the MaxEnt technique is capable of robust and accurate reconstructions of images from acoustic survey data with skewed distributions. Specifically, a statistical hypothesis test (Syrjala, 1996) failed to find significant difference spatially between the original simulated data and a best reconstruction of that data, chosen based on the evidence value, and generated from a virtual

Table 2: A selection of statistics relating to the reconstructions shown in Figures 3 and 4. The highlighted columns show the reconstruction chosen, based on the highest evidence.

Channels	Weighting	Evidence	Standard deviation	Mean value	Mean error	Max. value	Max. error	CV (%)	Biomass (million tonnes)
8	5	-12 595.1	101.6	17.4	5.5	5 657.1	191.3	26.8	42.81
8	6	-12 533.6	367.0	48.7	5.4	12 261.6	207.7	12.1	94.61
8	7	-12 508.0	994.7	99.5	4.9	43 606.5	209.2	4.9	207.98
8	8	-12 508.8	1 365.9	150.1	4.8	83 340.9	182.0	3.0	341.59
8	9	-12 512.3	2 074.7	225.8	4.9	130 628.3	161.8	2.0	500.50
8	10	-12 516.1	4 608.1	418.5	5.0	188 896.3	147.4	1.5	699.19
5	7	-13 123.4	250.0	10.2	1.3	925 329.7	68.5	6.3	88.44
6	7	-12 751.3	505.4	23.5	1.8	627 868.5	114.7	3.4	218.79
7	7	-12 561.4	20 604.3	464.1	2.6	3 637 959.7	81.9	0.8	1 290.40
8	7	-12 508.0	994.7	99.5	4.9	43 606.5	209.2	4.9	207.98
9	7	-12 546.9	59.2	8.7	13.3	1 011.8	104.5	157.1	6.12

Table 3: Biomass estimates for SSMUs in CCAMLR Area 48.

Survey	SSMU	Area	Mean density		Max. density		Biomass (MaxEnt) (million tonnes)	Biomass (Hewitt, 2004a) (million tonnes)	CV (MaxEnt) (%)
			Mean density (MaxEnt) $\text{g m}^{-2}$	Mean density (Hewitt, 2004a) $\text{g m}^{-2}$	Max density (MaxEnt) $\text{g m}^{-2}$	Max density (Hewitt, 2004a) $\text{g m}^{-2}$			
Entire reconstruction			60.4		23 832.7				
			101.1		43 569.5				
APPA	1		134.9	11.2	28 558.9	65.192	5.414	5.1	
APW	2		20.5	37.7	237.6	0.753	1.384	70.9	
APDPW	3		2 270.5	37.7	28 558.9	35.874	0.596	2.4	
APDPE	4		24.2	37.7	1 990.3	0.397	0.618	16.2	
APBSW	5		7.6	37.7	89.6	0.167	0.829	336.5	
APBSE	6		48.1	37.7	2 306.2	1.381	1.082	2.7	
APEI	7		302.4	37.7	8 195.3	10.946	1.365	0.8	
APE	8		0.0	37.7	0.3	0.003	2.322	655.5	
SOPA	9		38.1	24.5	4 886.0	30.799	19.816	16.5	
SOW	10		61.4	150.4	947.2	0.988	2.421	17.4	
SONE	11		0.5	150.4	6.4	0.005	1.624	8 751.1	
SOSE	12		15.7	150.4	136.4	0.243	2.331	274.5	
SGPA	13		61.7	24.5	5 385.9	57.194	22.721	3.5	
SGW	14		40.7	39.3	612.5	1.742	1.682	1.2	
SGE	15		64.4	39.3	2 998.6	3.554	2.169	1.6	
Subarea 48.4	16		235.3	na	43 569.5	198.163	na	2.2	

survey which provided values for approximately 0.56% of the pixels, the same percentage as is available for the CCAMLR-2000 Survey reconstructions.

## Discussion and conclusion

The resulting 'best' reconstruction (Figure 5) exhibits a number of the desired qualities one might wish to see, and indeed which one might ordinarily be used to select the best reconstruction. It is reassuring that, using only the Bayesian evidence value, we have been led to choose this reconstruction. Firstly, the reconstruction does not show structure parallel to the original survey transects. Naturally, a failure to properly fill the gaps between transects would lead to an unsupported bias toward higher values on-transect than off-transect. Such transect-related structure was evident in krill reconstructions prepared in previous papers (Brierley et al., 2003; Wafy et al., 2003), and suggests that a further increase in the number of hidden channels would have improved their results. It is a minimum requirement of a plausible reconstruction that the gaps be filled; equally, any further smoothing beyond the point at which transect-related structure disappears would unnecessarily reduce the information content of the image. It is informative that as reconstructions with 6–9 hidden channels (Figure 3) are observed, the first image in which transect-related structure is not evident is at eight hidden channels, which corresponds to the highest evidence value. Furthermore, the excessive smoothing with nine hidden channels does indeed result in a fall in the evidence value.

Secondly, the result demonstrates that MaxEnt can assign density maxima off-transect (Figure 5, for example around 40°W 56°S). Certainly there is no reason to believe that the survey transects happened to pass through all the regions of highest krill density, so this behaviour is very welcome. Inevitably, the position and size of such maxima is only probabilistically determined from very limited data. However, since the use of the MaxEnt prior ensures that any structure in the reconstruction must be based on the data (Gull and Daniell, 1978; Gull and Skilling, 1991), some level of support for these off-transect maxima must exist within the dataset. This is a clear example of the spatial information which would be ignored by, and hence lost to, the conventional Jolly and Hampton (1990) approach.

Thirdly, the resulting total biomass estimate for the whole survey area of  $207.98 \pm 10.08$  million tonnes is plausible, compared with the Demer and Conti (2005) estimate of  $109.4 \pm 11.38$  million

tonnes generated from the same on-transect data values by the Jolly and Hampton (1990) method. The MaxEnt estimate is substantially larger, but not implausibly so, given the tiny number of data involved and the fact that higher off-transect densities are possible. There is considerable doubt about what lies between transects, and it is reasonable to expect different statistical analysis methods to produce different biomass estimates. One measure of support for this higher biomass estimate is that it accords much better with estimates that predator populations require a krill biomass of between 150–300 million tonnes to sustain them (Priddle et al., 1998; Smetacek and Nicol, 2005).

It is worth remembering that the CCAMLR-2000 Survey was designed specifically with the Jolly and Hampton (1990) approach in mind. Survey transects were pseudo-randomly placed within chosen strata, in accordance with the Jolly and Hampton formalism. Conversely, from a MaxEnt point of view, it would be more suitable to have the transects evenly spaced. Those regions where the transect spacing was as high as 175 km will inevitably present greater challenges to reconstruction than areas where the separation was as low as 75 km (or even lower, as in areas where extra survey effort was concentrated, for example to the north of South Georgia). The authors suggest that future surveys be designed on a regular grid.

Summary statistics of krill biomass are given in Table 3 for each of the SSMUs shown in Figure 1 and listed in Table 1. However, substantial parts of regions 1, 2, 8, 9, 13 and 16 lie outside the survey area. In these cases, the mean density, calculated over a small part of the SSMU, has to be applied to the whole SSMU to generate biomass estimates. It is likely that these mean densities are not representative of the whole SSMU, and hence the biomass estimates may not be reliable. For example, in Antarctic Peninsula East (SSMU 8) the biomass estimate of 0.003 million tonnes reflects the fact that very few krill were found in the tiny part of SSMU 8 that was in the survey area (in fact, although the survey bounds do encroach into SSMU 8, no actual transects do – see Figure 1). In the absence of more data, little can be done to better calculate biomass for such regions.

Hewitt et al. (2004b) took the mean for all SSMUs 2–8 (and 10–12, 14–15) and applied this to each of the individual areas (see Table 3). This is perhaps the best overall option available, particularly since Hewitt et al. (2004b) required solid figures to continue their analysis of possible catch limits, but may not provide the best answer for those SSMUs (e.g. 3, 4) where more data are available.

In this paper, all biomass estimates are reported as calculated, whilst accepting that some values are subject to severe uncertainty. What Table 3 indicates most clearly is the level of ignorance about these density and biomass values. Bearing in mind that data based on the Demer and Conti (2005) target-strength model were used, which led to a biomass estimate about 2.5 times larger than previous estimates (Hewitt et al., 2002), it is fair to assume that the SSMU biomass and mean density estimates from Hewitt et al. (2004b) are also underestimates. However, the MaxEnt biomass estimates are sometimes appreciably lower than those reported in Hewitt et al. (2004b) calculated using the Jolly and Hampton (1990) method, even in regions (e.g. 10–12) with reasonable survey coverage. It seems that any putative ‘best estimate’ of biomass in SSMUs is subject to enormous uncertainty, and estimates from the CCAMLR-2000 Survey data may not lead to good decisions about catch limits in these regions. The application of the ‘precautionary principle’ would suggest that, in this state of relative ignorance, catch limits for at least some of the SSMUs should be set at extremely low levels.

In addition to generating biomass estimates, the second stated ambition of this research is to generate accurate, useful maps of krill distribution. Figures 5 and 6 show the MaxEnt reconstruction and an estimated map taken from Hewitt et al. (2004a). There are clear differences between these maps. The question of which map better represents the actual krill distribution is hard to resolve in the absence of more data. Hewitt et al. (2004a) offer only a very short paragraph to explain how their map was created, since that paper was much more concerned with estimating krill biomass than with mapping dispersion. It is of course not impossible that the map in Hewitt et al. (2004a) is more correct than the MaxEnt map, but this analysis provides reason to believe the MaxEnt solution to be more probable. The MaxEnt solution is very likely to be the most accurate map yet published from the CCAMLR-2000 Survey data.

Any map from which biological or stock-management inferences are to be drawn should be very carefully considered, since situations of sparse data allow so many different possible maps to be consistent with that data. It is further suggested that the MaxEnt formalism, with its preference for smoothness and its sound probabilistic basis, is a useful framework for refining the best estimates presented here.

The errors calculated for the reconstruction, shown in Figure 7, do not exhibit large amounts of unwanted structure. High values of standard

deviation are generally found only where there are high density values, and thus represent small percentage errors. The exception is to the west of the South Orkney Islands. In terms of the MaxEnt calculations, this means that there are large variations in the density estimates in this area between the chosen solution and almost-as-probable candidate solutions. This may be due to a lack of information in the local data; at this time this error peak cannot be fully explained. It is possible that approximations in the algorithm, used to overcome intractability in some of the calculations, are less than sufficiently accurate for data in this region.

There are undoubtedly improvements still to be made to the reconstruction algorithm used here. Specifically, the Gaussian blurring function is used simply for ease of computation and has no particular basis in biology. One of the main aims of this research in the coming months is to redress this situation. Since the MaxEnt formalism treats the blurring function as entirely separate from the MaxEnt prior distribution, it can be adjusted without fear of compromising the validity of the technique. In fact, different blurring functions will produce different evidence values, and selection between alternative functions becomes just another exercise in parameter estimation. As a first step, future investigations will use different blurring widths in different directions, allowing better reconstruction of data exhibiting significant anisotropy, the effects of which have not been closely considered in this paper.

Another possible route to better estimates could be found by using more information that is external to the dataset in question. Any information derived from a survey cannot be used to define a prior for analysis of that survey, since such an idea is obviously circular; however, information from other sources, other surveys or experiments may legitimately form part of the prior information for an analysis. There is a relatively straightforward way to include such information in the formalism. Currently, a uniform first trial image is used (see ‘Calculating the quantified MaxEnt result’ above), since no prior knowledge of the distribution of the species is claimed. However, there may be relevant knowledge available – for example, a known relationship between water depth and species density. In such circumstances, basing the first ‘guess’ on some function of the bathymetry of the survey area may be justified. In a very simple case, for example where species density could be thought to be approximately linearly related to water depth, the starting trial image would simply consist of the water depth in each cell of the survey area scaled by an appropriate constant. It should be noted that the

MaxEnt prior distribution was a formula expressing the relative belief in different possible prior images – whether starting from a uniform or non-uniform trial image, that formula still expresses the expectations about the relative probability of changes to that trial image made after comparison to the data.

In the case of krill, there is evidence (Trathan et al., 2003) that krill density is normally significantly higher in on-shelf than in off-shelf regions. Using this information, we can choose a first trial image, based on the bathymetry of the area, with very low density values in off-shelf areas. This starting image would then ensure a bias towards higher on-shelf densities that may not be deducible from the CCAMLR-2000 Survey data directly, but which can be predicted based on other available information. This can reasonably be expected to further refine the estimates of krill biomass and density distribution, and is a logical next step for this research. The ability to make use of such external information represents one of the strengths of the MaxEnt formalism.

One of the aims of this paper has been to consider the possible advantages of MaxEnt as an alternative to kriging and to Jolly and Hampton (1990) analyses. In reference to kriging, the use of the evidence value offers a chance to objectively compare competing MaxEnt reconstructions in a way that is not always available when comparing, for example, reconstructions from two different types of kriging. Additionally, the possibility of including external information, such as bathymetry, may represent a far bigger advantage over traditional geostatistics.

With respect to the Jolly and Hampton (1990) method, the obvious advantage of MaxEnt is in making use of the spatial information contained in the data. This advantage may not be pronounced in this study, due to the enormous transect spacing of the CCAMLR-2000 Survey, but can be expected to be more crucial for smaller-scale surveys such as those studied by Brierley et al. (2003).

In conclusion, the authors believe that the MaxEnt procedure shows significant promise as a reconstruction technique, and also as an alternative to the Jolly and Hampton (1990) method of calculating total regional biomass from acoustic survey data. The CCAMLR-2000 Survey data is a particularly strong challenge for the algorithm, but it so far appears that plausible reconstructions are possible. The attempts to generate biomass results demonstrate the shortage of data in certain SSMUs. This should emphasise that, regardless of apparent errors calculated by this method or by the Jolly and Hampton (1990) method, enormous uncertainty

exists in these biomass estimates, and this must be taken into account when setting allowable catch limits.

## Acknowledgements

Thanks to David Demer for the original on-transect data, Eric Appleyard for the SSMU coordinates, Cairistiona Anderson and Claire Waluda for providing the coordinates of the survey bounds, and John Simmonds for the North Sea herring mock data used to test the veracity of MaxEnt reconstructions from line-transect survey data.

## References

- Bayes, T. 1763. An essay towards solving a problem in the doctrine of chances. *Philos. Trans. Roy. Soc. Lond.*, 53: 370–418.
- Brierley, A.S., S.F. Gull and M.H. Wafy. 2003. Bayesian Maximum Entropy reconstruction of stock distribution and inference of stock density from line-transect acoustic survey data. *ICES J. Mar. Sci.*, 60 (3): 446–452.
- Charter, M.K. and S.F. Gull. 1991. Maximum Entropy and drug absorption. *Journal of Pharmacokinetics and Biopharmaceutics*, 19 (5): 497–520.
- Clark, J.S. 2005. Why environmental scientists are becoming Bayesians. *Ecology Letters*, 8 (1): 2–14.
- Cox, R.T. 1946. Probability, frequency and reasonable expectation. *Am. J. Phys.*, 14: 1–13.
- Demer, D.A. 2004. An estimate of error for CCAMLR-2000 Survey estimate of krill biomass. *Deep-Sea Res., II*, 51: 1237–1251.
- Demer, D.A. and S.G. Conti. 2005. New target-strength model indicates more krill in the Southern Ocean. *ICES J. Mar. Sci.*, 62: 25–32.
- Gull, S.F. and G.F. Daniell. 1978. Image reconstruction from incomplete and noisy data. *Nature*, 272: 686–690.
- Gull, S.F. and J. Skilling. 1991. Quantified Maximum Entropy. *MemSys5: Users Manual*. [www.max-ent.co.uk/documents/MemSys5\\_manual.pdf](http://www.max-ent.co.uk/documents/MemSys5_manual.pdf).
- Hewitt, R.P., J.L. Watkins, M. Naganobu, P. Tshernyshkov, A.S. Brierley, D.A. Demer, S. Kasatkina, Y. Takao, C. Goss, A. Malyshko, M.A. Brandon, S. Kawaguchi, V. Siegel,

- P.N. Trathan, J.H. Emery, I. Everson and D.G.M. Miller. 2002. Setting a precautionary catch limit for Antarctic krill. *Oceanography*, 15 (3): 26–33.
- Hewitt, R.P., J. Watkins, M. Naganobu, V. Sushin, A.S. Brierley, D. Demer, S. Kasatkina, Y. Takao, C. Goss, A. Malyshko, M. Brandon, S. Kawaguchi, V. Siegel, P. Trathan, J. Emery, I. Everson and D. Miller. 2004a. Biomass of Antarctic krill in the Scotia Sea in January/February 2000 and its use in revising an estimate of precautionary yield. *Deep-Sea Res., II*, 51: 1215–1236.
- Hewitt, R.P., G. Watters, P.N. Trathan, J.P. Croxall, M.E. Goebel, D. Ramm, K. Reid, W.Z. Trivelpiece and J.L. Watkins. 2004b. Options for allocating the precautionary catch limit of krill among small-scale management units in the Scotia Sea. *CCAMLR Science*, 11: 81–97.
- Jaynes, E.T. 1978. Where do we stand on Maximum Entropy? In: Rosenkrantz, R. (Ed.). *Papers on Probability, Statistics and Statistical Physics*. Reidel, Dordrecht: 211–314.
- Jaynes, E.T. 2003. *Probability Theory: the Logic of Science*. Cambridge University Press, Cambridge.
- Johnson, R.W. and J.E. Shore. 1980. Axiomatic derivation of the principle of Maximum Entropy and the principle of Minimum Cross Entropy. *IEEE Transactions on Information Theory*, 26: 26.
- Johnson, R.W. and J.E. Shore. 1983. Axiomatic derivation of the principle of Maximum-Entropy and the principle of Minimum Cross-Entropy – comments and correction. *IEEE Transactions on Information Theory*, 29 (6): 942–943.
- Jolly, G.M. and I. Hampton. 1990. A stratified random transect design for acoustic surveys of fish stocks. *Can. J. Fish Aquat. Sci.*, 47: 1282–1291.
- Lizamore, S.C. 1995. Topics in Maximum Entropy applications. M.Sc. thesis, Victoria University of Wellington, 66 pp.
- Maravelias, C.D., D.G. Reid, E.J. Simmonds and J. Haralabous. 1996. Spatial analysis and mapping of acoustic survey data in the presence of high local variability: geostatistical application to North Sea herring (*Clupea harengus*). *Can. J. Fish. Aquat. Sci.*, 53 (7): 1497–1505.
- Priddle, J., I.L. Boyd, M.J. Whitehouse, E.J. Murphy and J.P. Croxall. 1998. Estimates of Southern Ocean primary production – constraints from predator carbon demand and nutrient draw-down. *J. Mar. Sys.*, 17 (1–4): 275–288.
- Rivoirard, J., E.J. Simmonds, K.G. Foote, P.G. Fernandes and N. Bez. 2000. *Geostatistics for Estimating Fish Abundance*. Blackwell: 198 pp.
- Sivia, D.S. 1996. *Data Analysis – a Bayesian Tutorial*. Oxford University Press: 189 pp.
- Skilling, J. 1988a. The axioms of maximum entropy. In: Erickson, G.J. and C.R. Smith (Eds). *Maximum Entropy and Bayesian Methods in Science and Engineering*. Kluwer, Dordrecht: 1 p.
- Skilling, J. 1988b. Classic Maximum Entropy. In: Skilling, J. (Ed.). *Maximum Entropy and Bayesian Methods*. Kluwer Academic Press, Cambridge: 45–52.
- Skilling, J. 1991. Bayesian reasoning. *Nature*, 353 (6346): 707–708.
- Skilling, J. 1992. Quantified Maximum-Entropy. *American Laboratory*, 24 (15): J32–M32.
- Skilling, J. and S.F. Gull. 1989. *Bayesian Maximum Entropy*. Proceedings of the AMS-IMS-SIAM Conference on Spatial Statistics and Imaging, Bowdoin College, Maine, 1988.
- Skilling, J. and S. Sibisi. 1990. Fundamentals of MaxEnt in Data Analysis. *Institute of Physics Conference Series*, 107: 1–21.
- Smetacek, V. and S. Nicol. 2005. Polar ocean ecosystems in a changing world. *Nature*, 437 (7057): 362–368.
- Syrjala, S.E. 1996. A statistical test for a difference between the spatial distributions of two populations. *Ecology*, 77 (1): 75–80.
- Tikochinsky, Y., N.Z. Tishby and R.D. Levine. 1984. Consistent inference of probabilities for reproducible experiments. *Physical Review Letters*, 52 (16): 1357–1360.
- Trathan, P.N., J.L. Watkins, A.W.A. Murray, A.S. Brierley, I. Everson, C. Goss, J. Priddle, K. Reid, P. Ward, R. Hewitt, D. Demer, M. Naganobu, S. Kawaguchi, V. Sushin, S.M. Kasatkina, S. Hedley, S. Kim and T. Pauly. 2001. The

CCAMLR-2000 Krill Synoptic Survey: a description of the rationale and design. *CCAMLR Science*, 8: 1–24.

Trathan, P.N., A.S. Brierley, M.A. Brandon, D.G. Bone, C. Goss, S.A. Grant, E.J. Murphy and J.L. Watkins. 2003. Oceanographic variability and changes in Antarctic krill (*Euphausia superba*) abundance at South Georgia. *Fish. Oceanogr.*, 12 (6): 569–583.

Wafy, M.H., A.S. Brierley, S.F. Gull and J.L. Watkins. 2003. Maximum Entropy reconstructions of krill

distribution and estimates of krill density from acoustic surveys at South Georgia, 1996–2000. *CCAMLR Science*, 10: 91–100.

Weber, L.H., S.Z. El-Sayed and I. Hampton. 1986. The variance spectra of phytoplankton, krill and water temperature in the Antarctic Ocean south of Africa. *Deep-Sea Res.*, 33 (10): 1327–1343.

Weir, N. and S. Djorgovski. 1991. High-resolution imaging of the double QSO 2345+007. *Astronomical Journal*, 101 (1): 66–70.

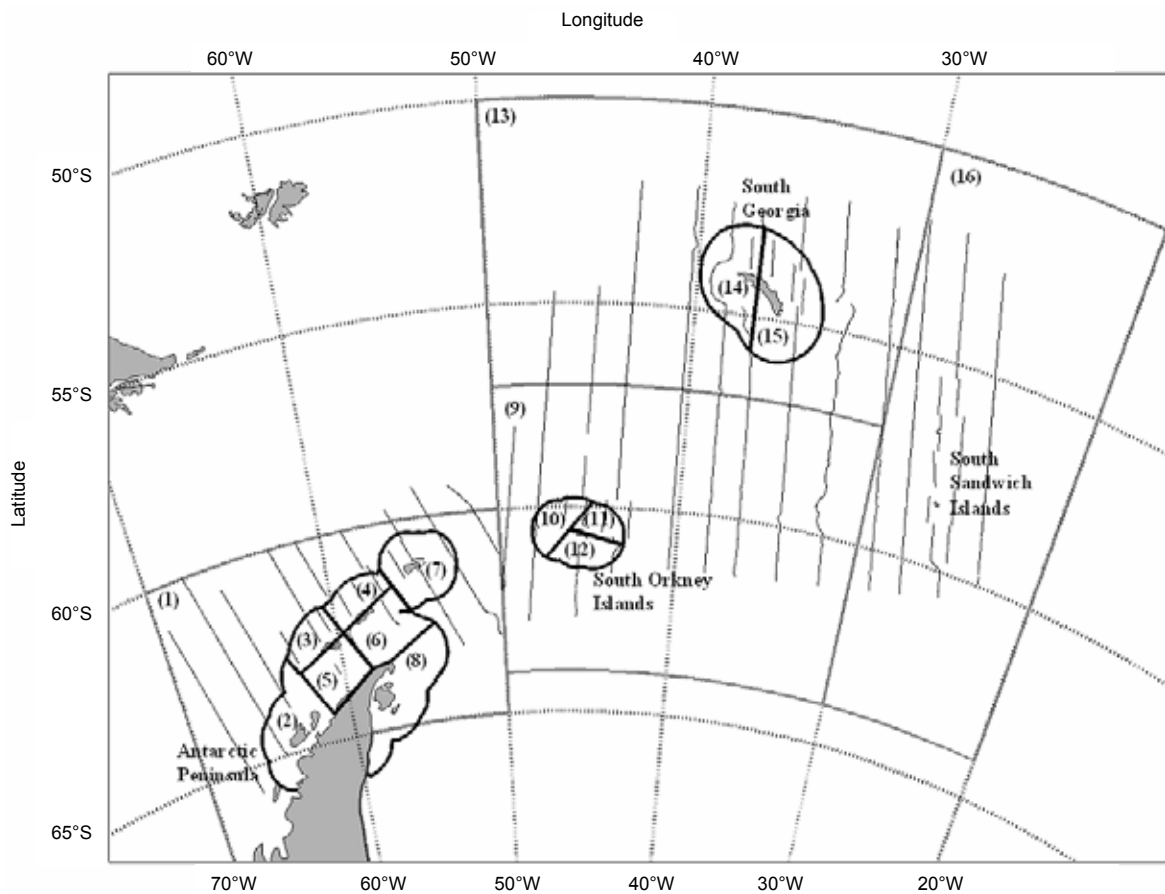


Figure 1: Small-scale management units (CCAMLR Subareas 48.1 to 48.4 as solid grey lines; smaller SSMUs in black) in CCAMLR Area 48, numbered following Hewitt et al. (2004b), and the CCAMLR-2000 Survey transects.

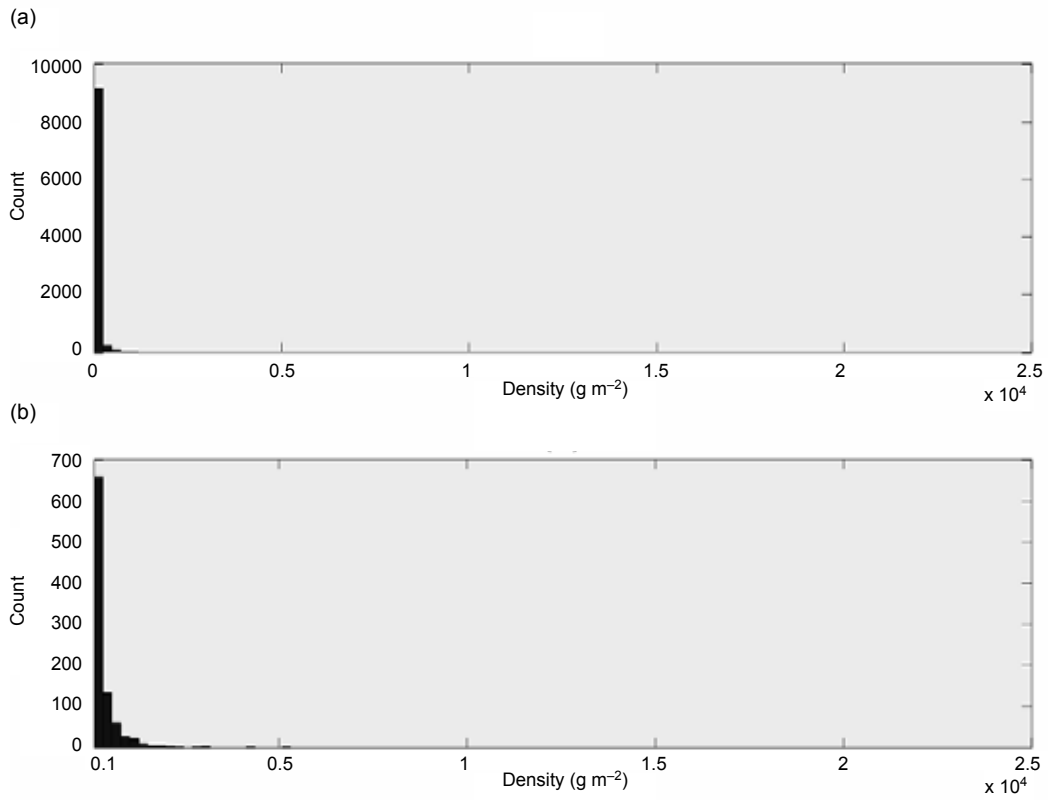


Figure 2: Histograms of density ( $\text{g m}^{-2}$ ) from the CCAMLR-2000 Survey, showing the extreme skewedness of the data: (a) all data; (b) only those density values over  $100 \text{ g m}^{-2}$ , demonstrating that the skewedness is inherent throughout the distribution and not just created by a large number of zeros.

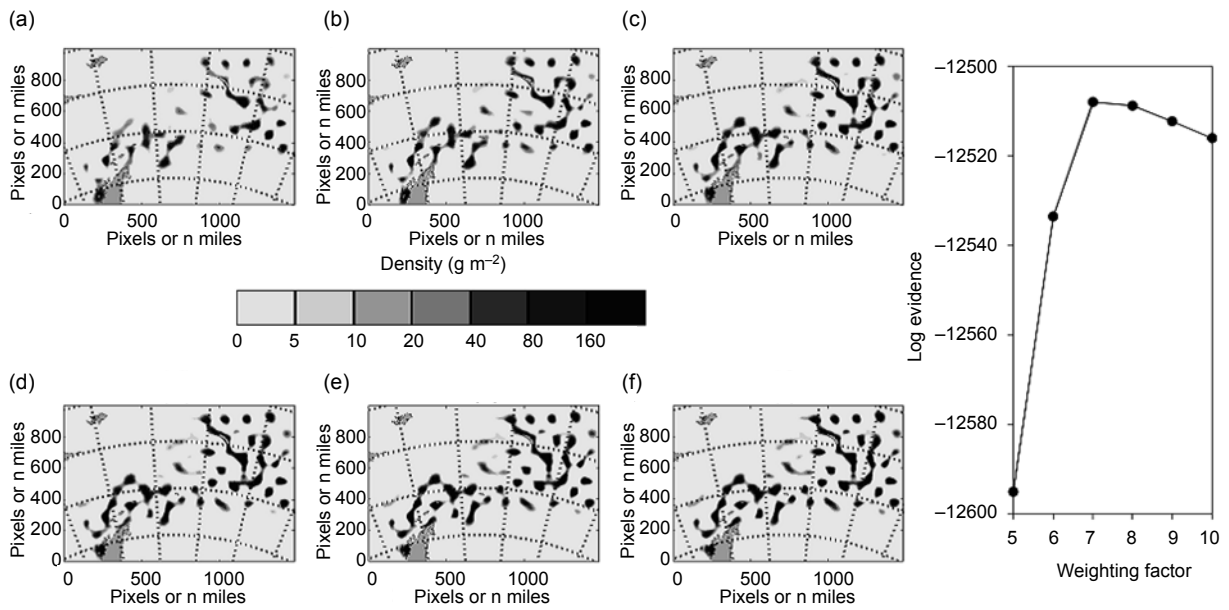


Figure 3: Reconstructions with values of (a) 5, (b) 6, (c) 7, (d) 8, (e) 9 and (f) 10 for the weighting factor. The associated graph shows the highest evidence to be associated with (c).

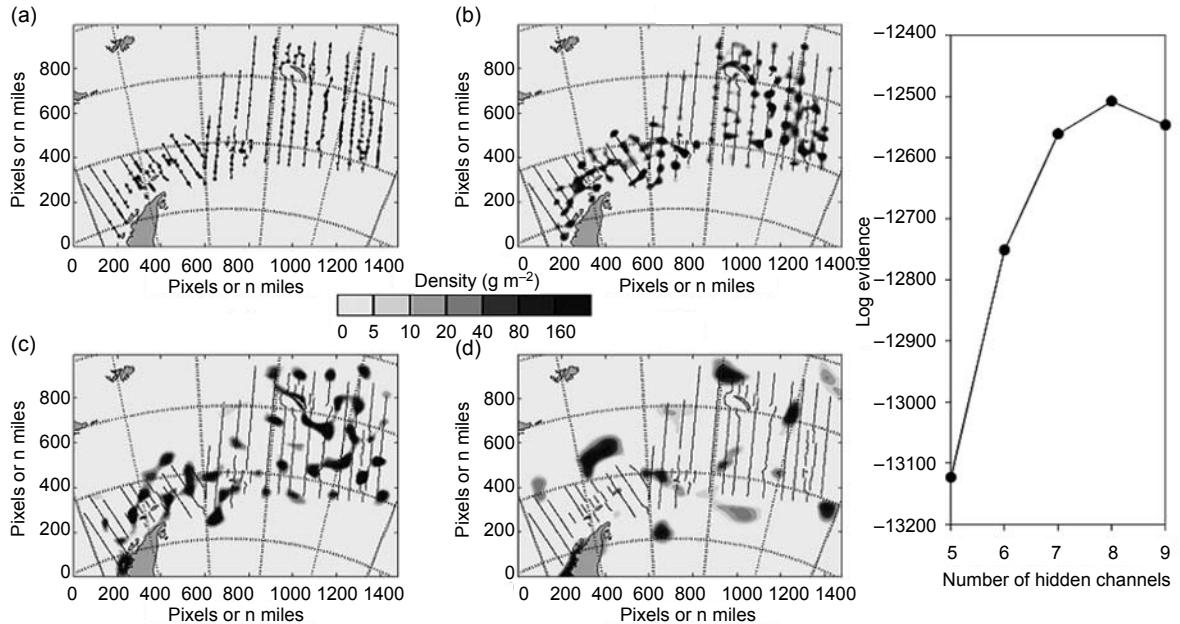


Figure 4: Reconstructions with (a) 6, (b) 7, (c) 8 and (d) 9 hidden channels. The associated graph shows the highest evidence to be associated with (c).

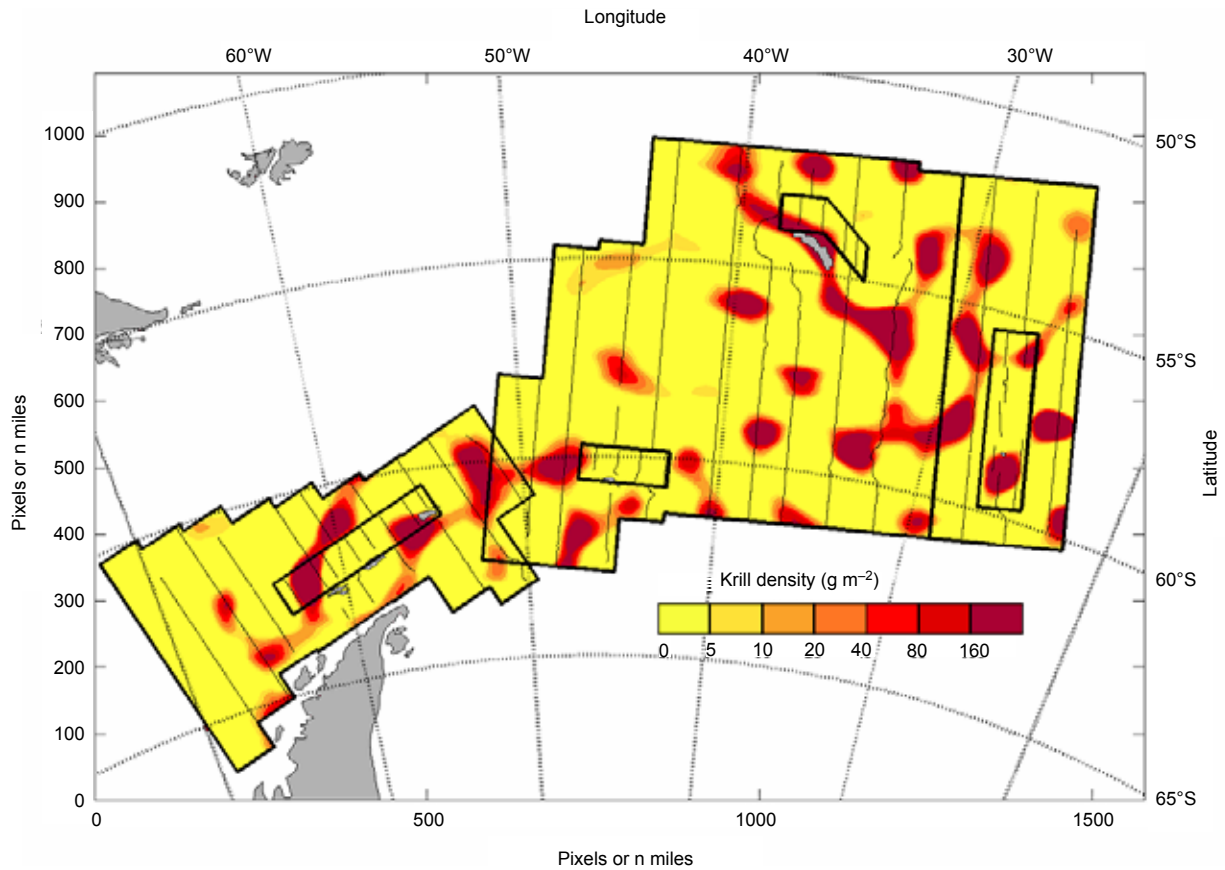


Figure 5: The MaxEnt result, with the bounds (thick lines) and transects (thin lines) of the CCAMLR-2000 Survey. The colour scale is chosen to facilitate comparison with Figure 6.

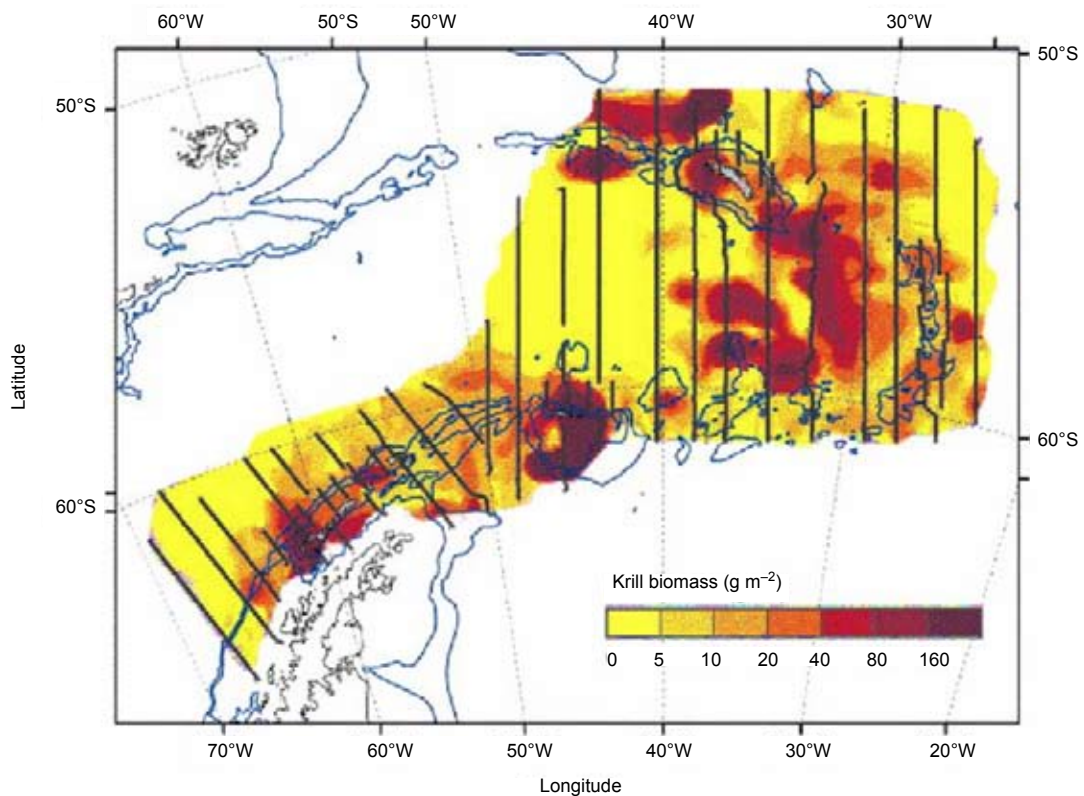


Figure 6: An estimate of krill density distribution from the CCAMLR-2000 Survey, shown in approximately the same colour scale as the MaxEnt reconstructions, reprinted with permission from Hewitt et al. (2004a).

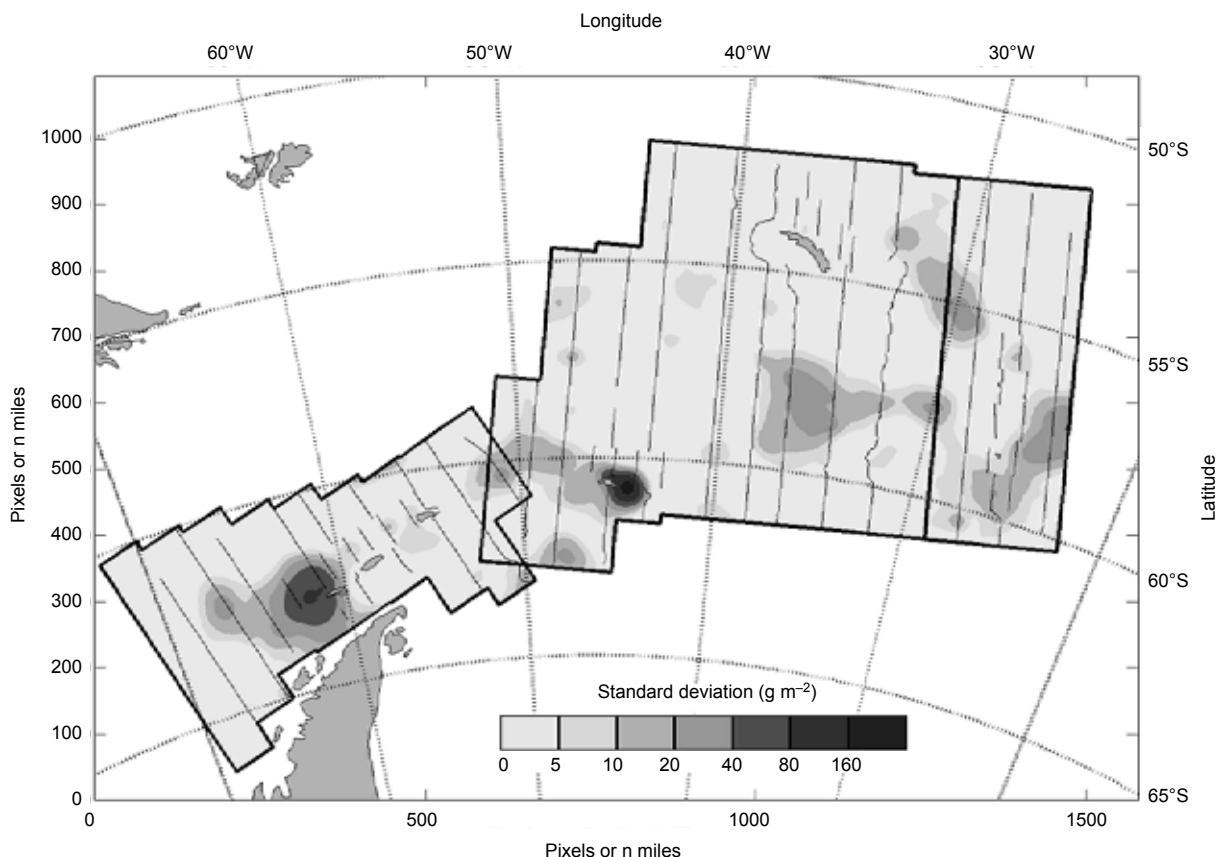


Figure 7: The calculated standard deviation for the pixels of the chosen MaxEnt reconstruction, with the survey transects overlaid.

#### Liste des tableaux

- Tableau 1: Liste des SSMU.
- Tableau 2: Sélection de statistiques relatives aux reconstructions illustrées aux figures 3 et 4. Les colonnes surlignées indiquent la reconstruction retenue, à partir de l'évidence la plus grande.
- Tableau 3: Estimations de la biomasse des SSMU de la zone 48 de la CCAMLR.

#### Liste des figures

- Figure 1: Unités de gestion à petite échelle (sous-zones 48.1 à 48.4 de la CCAMLR en traits pleins gris ; SSMU plus petites en noir) de la zone 48 de la CCAMLR, numérotées d'après Hewitt et al. (2004b) et transects de la campagne CCAMLR-2000.
- Figure 2: Histogrammes de densité ( $\text{g m}^{-2}$ ) tirés de la campagne CCAMLR-2000 illustrant le biais extrême des données : (a) toutes les données, (b) uniquement les données de densité supérieures à  $100 \text{ g m}^{-2}$  pour démontrer que le biais est inhérent à l'ensemble de la distribution et ne provient pas simplement du grand nombre de zéros.
- Figure 3: Reconstructions avec (a) 5, (b) 6, (c) 7, (d) 8, (e) 9 et (f) 10 comme facteur de pondération. Le graphique correspondant montre que l'évidence la plus grande est associée à (c).
- Figure 4: Reconstructions avec des canaux cachés de (a) 6, (b) 7, (c) 8 et (d) 9. Le graphique correspondant montre que l'évidence la plus grande est associée à (c).

- Figure 5: Résultat de MaxEnt, avec les limites (traits épais) et les transects (traits fins) de la campagne CCAMLR-2000. Les couleurs ont été choisies pour faciliter la comparaison avec la figure 6.
- Figure 6: Estimation de la distribution de la densité de krill d'après la campagne CCAMLR-2000, illustrée avec des couleurs pratiquement identiques aux reconstructions de MaxEnt, et republiée avec l'autorisation de Hewitt et al. (2004a).
- Figure 7: Ecart-type calculé pour les pixels de la reconstruction MaxEnt sélectionnée.

#### Список таблиц

- Табл. 1: Список обозначений SSMU.
- Табл. 2: Набор статистических показателей, связанных с реконструкцией, показанной на рис. 3 и 4. Выделенные столбцы показывают выбранную реконструкцию на основе наивысшего критерия свидетельства.
- Табл. 3: Оценки биомассы по SSMU Района 48 АНТКОМа.

#### Список рисунков

- Рис. 1: Мелкомасштабные единицы управления (подрайоны АНТКОМа 48.1–48.4 – как сплошные серые линии, более мелкие SSMU показаны черным) в Районе 48 АНТКОМа, пронумерованные в соответствии с работой Hewitt et al. (2004b), и разрезы съемки АНТКОМ-2000.
- Рис. 2: Гистограммы плотности ( $\text{г м}^{-2}$ ) по съемке АНТКОМ-2000, демонстрирующие крайнюю смещенность данных: (a) всех данных; (b) только значений плотности свыше  $100 \text{ г м}^{-2}$  и показывающие, что смещенность присуща всему распределению, а не является просто результатом большого числа нулей.
- Рис. 3: Реконструкции со значениями весового коэффициента (a) 5, (b) 6, (c) 7, (d) 8, (e) 9 и (f) 10. Приведенный график показывает, что наивысший критерий свидетельства связан с (c).
- Рис. 4: Реконструкции с (a) 6, (b) 7, (c) 8 и (d) 9 скрытыми каналами. Приведенный график показывает, что наивысший критерий свидетельства связан с (c).
- Рис. 5: Результат MaxEnt с границами (жирные линии) и разрезами (тонкие линии) съемки АНТКОМ-2000. Цветовая шкала выбрана так, чтобы проще было провести сравнение с рис. 6.
- Рис. 6: Оценка распределения плотности криля по съемке АНТКОМ-2000, показанная примерно в той же цветовой шкале, что и реконструкции MaxEnt; перепечатано с разрешения Хьюитта и др. (Hewitt et al., 2004a).
- Рис. 7: Рассчитанное стандартное отклонение для пикселей выбранной реконструкции MaxEnt с изображением разрезов съемки.

#### Lista de las tablas

- Tabla 1: Lista de las UOPE designadas.
- Tabla 2: Selección de las estadísticas pertinentes a las reconstrucciones mostradas en las figuras 3 y 4. Las hileras sombreadas muestran la reconstrucción elegida, basada en la evidencia más fehaciente.
- Tabla 3: Estimaciones de la biomasa por UOPE en el Área 48 de la CCRVMA.

### Lista de las figuras

- Figura 1: Unidades de ordenación en pequeña escala en el Área 48 de la CCRVMA (las Subáreas 48.1 a la 48.4 de la CCRVMA se muestran como líneas grises sólidas; las UOPE más pequeñas en líneas negras), numeradas como en Hewitt et al. (2004b); y transectos de la prospección CCAMLR-2000.
- Figura 2: Histogramas de la densidad ( $\text{g m}^{-2}$ ) de la prospección CCAMLR-2000, mostrando la extrema asimetría de los datos: (a) todos los datos; (b) solamente los valores de densidad por sobre  $100 \text{ g m}^{-2}$ , demostrando que la asimetría es inherente en toda la distribución y no creada por un gran número de ceros.
- Figura 3: Reconstrucciones con valores de (a) 5, (b) 6, (c) 7, (d) 8, (e) 9 y (f) 10 para el factor de ponderación. El gráfico correspondiente demuestra que la evidencia más fehaciente es la de (c).
- Figura 4: Reconstrucciones con (a) 6, (b) 7, (c) 8 y (d) 9 reconstrucciones ocultas. El gráfico correspondiente demuestra que la evidencia más fehaciente es la de (c).
- Figura 5: El resultado del método de MaxEnt, con los límites (líneas gruesas) y transectos (líneas delgadas) de la prospección CCAMLR-2000. La escala cromática fue elegida para facilitar la comparación con la figura 6.
- Figura 6: Estimación de la distribución de la densidad de kril de la prospección CCAMLR-2000, mostrada en los mismos colores que las reconstrucciones del método MaxEnt. La figura ha sido reproducida con autorización de los autores, Hewitt et al. (2004a).
- Figura 7: Desviación estándar calculada para los píxeles de la reconstrucción con el método MaxEnt seleccionada, y transectos de prospección superpuestos.